H2Open Journal

IWA PUBLISHING

H2Open Journal Vol 5 No 4, 691 doi: 10.2166/h2oj.2022.128

Flood susceptibility mapping in the Bilate catchment, Ethiopia

Muluneh Legesse Edamo[a], Kedir Bushira[b,*] and Tigistu Yisihak Ukumo[c]

[a] Faculty of Hydraulic and Water Resources Engineering, Arba Minch University, P.O. Box 21, Arba Minch, Ethiopia
[b] Faculty of Engineering, Department of Civil and Environmental Engineering, Namibia University of Science and Technology, Namibia
[c] Faculty of Water Resources and Irrigation Engineering, Arba Minch University, P.O. Box 21, Arba Minch, Ethiopia
*Corresponding author. E-mail: kdrmohammed@gmail.com

KB, 0000-0003-2049-0548

ABSTRACT

Flood susceptibility mapping plays a key role in planning flood mitigation. Floods may not be avoidable due to the future climate changes. The Bilate catchment in Ethiopia is vulnerable to flood disasters and it is used as case study in this project. The analytical hierarchy process (AHP) under multi-criteria decision analysis (MCDA) is used to develop the flood susceptibility map of the Bilate catchment. It was accordingly found that factors such as slope, rainfall, land use/land cover (LULC), elevation, topographic wetness index (TWI), soil type (ST), sediment transport index (STI), drainage density (DD), stream power index (SPI), and distance from the river (DR) have significant effects on the flood intensity in Bilate catchment. Each factor was evaluated by AHP, and an output map was developed in ARCGIS. The prepared flood susceptibility map was classified into five classes such as very low, low, moderate, high, and very high 9.3%, 32.6%, 41.2%, 10.8%, and 6.1% areas respectively. The flood susceptibility map reported in this research is a great resource for relevant parties, including government and non-governmental organizations, to evaluate the impacts of flooding in the Bilate catchment and throughout the nation. The flood identified in this research may also be used as a reference to flood-related studies.

Key words: AHP, climate change, flood-causing factors, flood risk, MCDA

HIGHLIGHTS

- Maps of flood susceptibility are created using proxy data and multi-criteria decision analysis (MCDA).
- The key elements that significantly contribute to the flood phenomenon are land use/land cover, rainfall, slope, and elevation.
- Flood susceptibility ranged from very high to very low throughout the whole Bilate catchment.
- An early warning system could make use of the flood susceptibility map produced in this study.

GRAPHICAL ABSTRACT

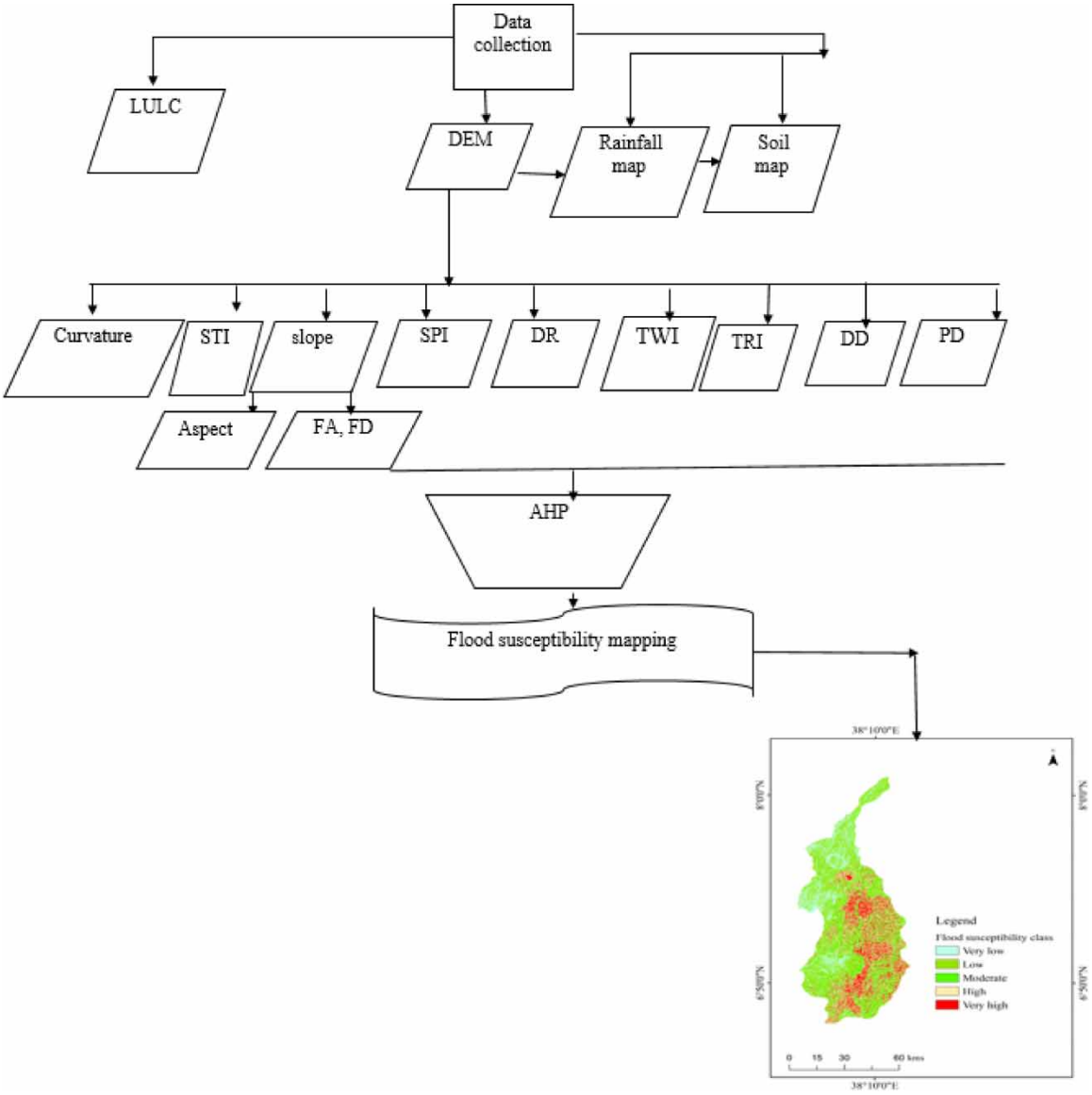

1. INTRODUCTION

Extreme hazards afflict both wealthy and poor countries creating massive financial disruptions, and major human sufferings (Hosseinzadehtalaei *et al.* 2021). Among other types of natural disasters such as volcanic eruptions, wildfires, explosions, and tsunamis, floods are the most frequent. It occurs in every corner of the planet (Das 2021). Floods have a lot of environmental and human consequences (Maskong 2019). Uncontrolled floods cause an overflow of water to destroy farming land, built environment, and infrastructure.

Flood susceptibility mapping is, however, necessary for identifying flood-prone areas to develop mitigation strategies (Antzoulatos *et al.* 2022). It helps to identify locations with flood susceptibility useful for effective flood risk management (Das 2018).

Flood can be predicted using hydraulic and hydrologic models. Hydraulic models such as MIKE, HEC-RAS, and SOBEK can simulate flood in one-dimensional (1D) or two-dimensional (2D) states (Teng *et al.* 2015; Malik *et al.* 2021). The hydrodynamic models can be used to create a physical framework for simulating various flows and sediment transport scenarios. The flood simulation models generally focus on river processes, taking overland processes as inputs of 1D or 2D hydrodynamic or hydrologic models. Due to the discrete structure of overland flow and unknown-dynamic boundary conditions, such classical approaches are not capable of

fast and reliable spatio-temporal estimations of overland flows, and require detailed and well-organized spatial data (Ozcelik & Gorokhovich 2020).

Hydrologic models are also used to study the water and sediment transport in a basin where excess water can be represented in the form of flood. However, from the various models and their respective accuracy and applicability, it can be concluded that there is no single best model because of the nature of environmental predictions. Every model can produce only an approximation of the reality it is attempting to illustrate (Galavi *et al.* 2013). Rather, there are many plausible solutions, depending on the purpose and needed complexity. Therefore, the practice of hydrologic modelling has, in general, included too much reliance on mathematics at the expense of true knowledge, and suffers from a need for a more rigorous evaluation of appropriateness. Typically, model selection tends to be more of a function of familiarity than appropriateness.

Many distributed models that have been developed over the years have gained popularity for their performance and capabilities. A few examples of such models are the MIKE SHE, TOPMODEL, and Soil and Water Assessment Tool (SWAT). Distributed hydrological models use a large number of parameters in simulating a watershed and accordingly are subjected to model uncertainty (Ayele *et al.* 2022; Edamo *et al.* 2022a, 2022b, 2022c; Ukumo *et al.* 2022a, 2022b). Although, their uncertainty can be quantified for real-world applications (Mirzaei *et al.* 2021), hydrological and hydraulic models do not suit the objectives of this study.

After all, the correct representation of flood propagation has proven to be a significant challenge for researchers and engineering experts all over the world, even on a small-scale watershed, due to the complicated natural processes (Di Baldassarre *et al.* 2010). The most comprehensive hydraulic models therefore must use simplification to simulate the flooding process. Consequently, the model accuracy is affected by assumptions (Ali 2018). Modelling approaches are restricted by the lack of data on ever-changing river sections and long-time hydrological observations (Edamo *et al.* 2022a, 2022b; Ukumo *et al.* 2022a, 2022b). A topographical method based on digital elevation models (DEMs) was developed in conjunction with the use of real-time predictive hydraulic models to improve large-scale awareness of flood risks (Ukumo *et al.* 2022a, 2022b). This may be a way to cope with the current flood mapping gaps, decrease the data dependency requirements, and promote hydraulic modelling and remote sensing applications. The scarcity of data in the Bilate catchment further limits its simulation (Kruczkiewicz *et al.* 2021).

Studies were conducted in various locations throughout the world to create an accurate flood susceptibility mapping method utilizing various decision-making and machine-learning methodologies via geospatial approaches. Edamo *et al.* (2022a, 2022b, 2022c) attempted to identify highly likely flood-prone zones using an analytical hierarchy process (AHP). Tehrany *et al.* (2014) used a weighted overlay analysis in geographic information system (GIS) to identify possible flood-prone areas in West Bengal, India. However, their weighted overlay method does not quantify each location's possibility of fitting to specific sets from numerous input rasters (Sepehri *et al.* 2020). Many academics have also adapted similar methods to quantify flood-prone zones using geospatial modelling (De Risi *et al.* 2018). Tehrany *et al.* (2014) used a machine-learning algorithm and numerous multivariate statistical methodologies to forecast flood susceptibility.

Experts from all around the world have recently emphasized the importance of cost- and time-effective decision-making approaches based on GIS techniques in flood mapping. The weights that have been assigned determine the precision of the AHP approach. It is worth noting, however, that various researchers in separate studies assign different weightings and rankings to different parameters. The availability of data for numerous elements, their quality, and geographical conditions all play a role in the effort to build a precise flood susceptibility map.

In this regard, multi-criteria decision analysis (MCDA) has been considered a suitable method to perform flood susceptibility mapping and evaluations as a result of its flexibility and the possibility of facilitating the dialogue between stakeholders, analysts, and scientists (Cinelli *et al.* 2014). The AHP is simple to understand and has a good software support. The MCDA method could be used to overcome the limitations of the hydrodynamic models (Odu 2019). As a result, the MCDA has gained widespread acceptance as a useful technique for assessing complicated choice issues (Abdel Hamid *et al.* 2020). One of the MCDA strategies is the AHP, which is a decision-making procedure that contains combining multiple-choice criteria into a hierarchy (Wind & Saaty 1980). One of the shortcomings of the AHP is the rejection of certainty in the spatial decision-making process (Singh *et al.* 2021). However, for flood susceptibility studies, the AHP is yet a viable option (Parsian *et al.* 2021).

Concluding from the reviewed literature and practiced methodologies, considering the limited data availability in Bilate, the MCDA approach is selected to map the flood-susceptible area in the catchment. However, an option

for assessing flood risk is to combine remote sensing and GIS tools with the AHP, particularly in areas with data scarcity (Mundhe 2019), and it is also followed here.

2. MATERIALS AND METHODS

2.1. Description of the study area

The Bilate catchment is one of the sub-basins of the Abaya-Chamo catchment of the Rift Valley Lake basin. It is located in the south-western part of Ethiopia. Bilate River is located approximately between 37.79° and 38.34°E longitudes and 6.56°–8.12°N latitudes (Figure 1). The catchment comprises an area of 5,625 km^2, stretching 338.9 km from north to south. Its elevation ranges between 1,174 and 3,324 m above mean sea level (Figure 1). The leptosols is the dominant type of soil in the Bilate watershed. The Bilate catchment has spring, summer, and winter climatic conditions. The catchment receives a significant amount of rainfall in the summer season. The summer season accounts for more than 93.2% of rainfall in the Bilate catchment.

2.2. Data sources

The data used in this study were collected from different sources. The rainfall data was obtained from the National Meteorological Agency of Ethiopia (NMAE) for the periods of 2010–2021. Soil was downloaded and used to prepare the soil map of the study area and supplied from the Food and Agriculture Organization (FAO). The source is https://www.fao.org/soils-portal/data-hub/soil-maps-and-databases/en/. The LULC data with resolution of 30 × 30 m was downloaded from United States Geological Survey (USGS): https://earthexplorer.usgs.gov/. Digital Elevation Model (DEM) with the resolution of 12.5 × 12.5 m were downloaded from Alaska satellite Facility (ASF): https://asf.alaska.edu/. The geology and geomorphology was obtained from Ministry of Water Irrigation and Energy of Ethiopia (MOWIEE).

2.3. Factors causing flood

The flood drivers are introduced in this section. Elevation, as the first factor, is the most critical characteristic of a basin that influences flood occurrence. Flooding is unlikely in high-elevation places, but it is more likely in lower-elevation areas. Water naturally flows from a higher point to a lower point. As elevation increases, the possibility of flooding decreases (Das & Pardeshi 2018; Ogato *et al.* 2020a). Flooding may occur more quickly in low-elevation locations than in higher-elevation places with a sharper slope.

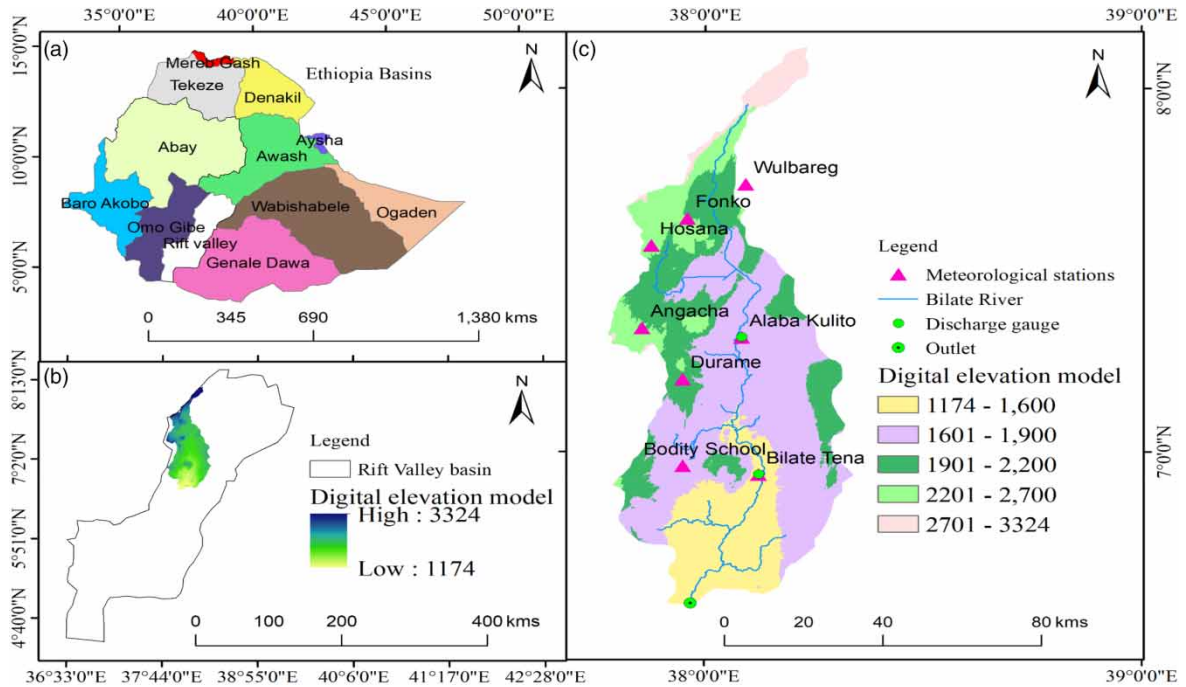

Figure 1 | Location maps of (a) basins in Ethiopia; (b) rift valley basin, and (c) the DEM.

Next, LULC is a key variable in predicting which areas have a high storm surge (Norman *et al.* 2010). In vegetated areas, flood threat is reduced due to the negative connection between flooding and green density. Storm runoff increases in residential areas and highways (Tehrany *et al.* 2013). The type of land used by sentient creatures as well as natural processes is displayed in the LULC pattern of an area (Ajin *et al.* 2013). Landscape management in the rural context offers a number of benefits in terms of environmental interactions. Changes in the land surface over time, as well as the effects of social and biological forces, must all be examined (Malik *et al.* 2021). These behaviours are regarded as catalysts for natural disasters that are catastrophic. Natural calamities such as floods are exacerbated by human actions such as deforestation and urbanization. Different forms of LULC might have a great effect on the water flow; for example, when bare land is present, rainwater runoff is often higher, whereas agricultural land or grass coverings hinder water overland flow and produce stagnation.

Soil type (ST): Soil parameters (permeability, soil layer thickness, rate of infiltration, and moistness of the soil prior to rain) have a direct impact on the rainfall–runoff process (Rimba *et al.* 2017). The ability of the soil to function as a sponge and absorb water will be influenced by its structure and infiltration capability. As soil infiltration capacity decreases, more surface runoff occurs, increasing the danger of flooding.

Slope and aspect: The slope is a key topographic feature in regulating the surface water flow in hydrology (Mojaddadi *et al.* 2017; Das *et al.* 2018). When the slope rises, the velocity of flow will also rise. A quick fall in the slope reduces infiltration but intensifies the surface runoff. The slope reduction stagnates large volume of water causing flooding. It is a crucial metric for surface zones that are extremely susceptible to flooding. One of the important criteria in defining whether or not a given rainfall will generate runoff is slope. The infiltration capacity of the soil is affected by the slope. The runoff increases because the soil does not have the time to absorb the water through its pore spaces. Slope and flood sensitivity are inversely related in that a steeper slope results in higher runoff and lower flood risk in that area. In contrast, in flat locations, the drainage rate is low and it causes water to stay on the surface of the ground and increases the level of the flood risk. When water is provided at a rate that exceeds the soil's capacity for infiltration, it rushes off the sloping terrain, causing flooding.

Another consideration is the aspect, which has an impact on the direction of flooding water flows as well as soil humidity (Cea & Costabile 2022). As a result, the feature has a secondary effect on flooding.

Rainfall: The reason for river flooding is mainly heavy rain; any water that does not enter the earth runs downstream as runoff. Excluding glacier portions, rain is the only origin of surface water. It has a tough link with river discharge and thus has a direct influence on the occurrence of floods. Flash floods in semi-arid locations can be triggered by unexpected rainfall.

Distance from the river (DR): The majority of flood-prone areas are typically situated along rivers. Because the distance from the river influences the frequency of floods and the river flow, it is an important criterion for identifying flood-prone areas in a catchment. The farther you are from the river, the less likely you are to get flooded (Liu *et al.* 2021).

Topographic Wetness Index (TWI): The TWI can be used to figure out how many topographic constraints there are on hydrological events in general. The TWI is inextricably related to the slope and upstream, contributing an orthogonal area per unit width to the flow direction. It is a real element (Kruczkiewicz *et al.* 2021) for the occurrence of floods, which spatially expresses the variation in the wetness of a basin. This index is generated to indicate the amount of water contained in each pixel of the region (Zhao *et al.* 2022) (Equation (1)):

$$\mathrm{TWI} = \ln \frac{\alpha}{\tan \beta} \tag{1}$$

where α is the upside slope (degree) and β is the slope gradient (in degree). In general, the high TWI values and flooding are strongly correlated with each other (Yang *et al.* 2021).

Sediment transport index (STI): This index increases the frequency of floods and cause foundation damage (Mehta *et al.* 2021) (Equation (2)):

$$\mathrm{STI} = \left(\frac{A}{22.13}\right)^{0.6} \left(\frac{\sin \beta}{0.0896}\right)^{1.3} \tag{2}$$

where β is the slope and A is the area of the catchment

Stream power index (SPI): It assesses the erosivity of rivers in a floodplain (Tehrany *et al.* 2014). The SPI is the primary driving force behind the channel progression throughout the river from the source to accumulation zone (Vilasan & Kapse 2022). Because of the higher stream power in the upstream stretch, the streams can erode and transfer a substantial amount of debris. When stream strength is reduced, the channels become shallow and shredded, resulting in sediment overbank deposition. The area with a low SPI class is usually susceptible to the flood the hydrologic system is hugely affected by the SPI. It refers to the bed's erodibility as well as its sediment transport potential (Chen *et al.* 2020) (Equation (3)):

$$\mathrm{SPI} = A \tan \beta \tag{3}$$

where A is the catchment area and β is the slope in radians.

Curvature: It is the degree to which a curve deviates from a straight line, or a curved surface deviates from a plane. Curvature describes the shape of the soil surface and reflects the capacity for water accumulation (Costache 2019). Curvature affects the flooding water budget. The negative value regions are involved in the runoff convergence operation (Towfiqul Islam *et al.* 2021). A positive value of curvature represents a convex surface, zero a flat surface, and a negative value a concave surface (Das 2019). The curvature splits the divergent and convergent runoff zones.

Flow accumulation (FA): Flow accumulation was calculated using the flow direction raster. Every column in the flow accumulation raster is awarded a discharge profile based on the number of cells that flow into it. An increase in flood sensitivity should, in this case, be accompanied by an increase in flow accumulation (Abdel Hamid *et al.* 2020).

Flow direction (FD): The ability to discern the flow direction of each raster pixel is one of a surface's hydrologic properties. The flow direction is a grid whose value represents each cell's steepest point in terms of flow direction.

Terrain ruggedness index (TRI): It measures the uniformity in the topographic distribution of altitude (Riley *et al.* 1999). This technique is quite useful for determining whether a region is flat or rugged (Das 2021). Because of their flat nature, regions with a low TRI rating have a greater risk of flooding. Therefore, very low TRI values can be found in flood plain.

Population density (PD): Population density affects the occurrence of flood. It is understood that the higher the amount of flood protection, the larger the growth in population density and the number of assets vulnerable to flooding over the last few decades (Bibi *et al.* 2019). If the population is densely distributed over the given area, the more prone it is to floods (Ogato *et al.* 2020b). Population growth increases the possibility of flooding as well as its potential effects by putting more pressure on drainage systems and encouraging urban development in flood-prone areas (Kablan *et al.* 2017). The rising sea levels and changing rainfall patterns are expected to make floods more frequent and intense over the coming decades. The flood occurrence and intensity will increase due to climate change and the increasing population The world's impoverished are particularly at risk of flooding and susceptible to its effects. The population data of the study area were collected from Central Statistical Agency of Ethiopia. The average population density calculation method was used to calculate the number of people per square kilometre.

Drainage density (DD): In general, the density of drainage increases with decrease in infiltration capacity of soil. The DD layer of the basin was produced in ArcGIS using line density tool. DD is calculated using the formula: $\mathrm{DD} = L/A$, where L is the length of the drainage channel in the catchment (km); A is the area of the watershed (km^2) (Ouma & Tateishi 2014).

Surficial geology (SG): Deals with the Earth's resources, their structure, and the processes that operate on them (Das 2019). The surficial geology includes drainage feature (pattern, density, etc.) and parent rock. The surficial geology affects the catchment runoff by formation of different permeable and impermeable rocks.

Geomorphology: The scientific study of landforms and the processes that shape them is known as geomorphology (Das 2019).

The identifying flood-influencing factors helps in flood risk management reduce the flood damage in the Bilate catchment. LULC has a great impact runoff (16.80%) in the Bilate catchment (Figure 2).

2.4. Analytical hierarchy process

An AHP is a simple decision-making strategy that considers the relative importance of numerous elements (Németh *et al.* 2019). It combines multiple-choice criteria into a hierarchy, comparing numerous options for

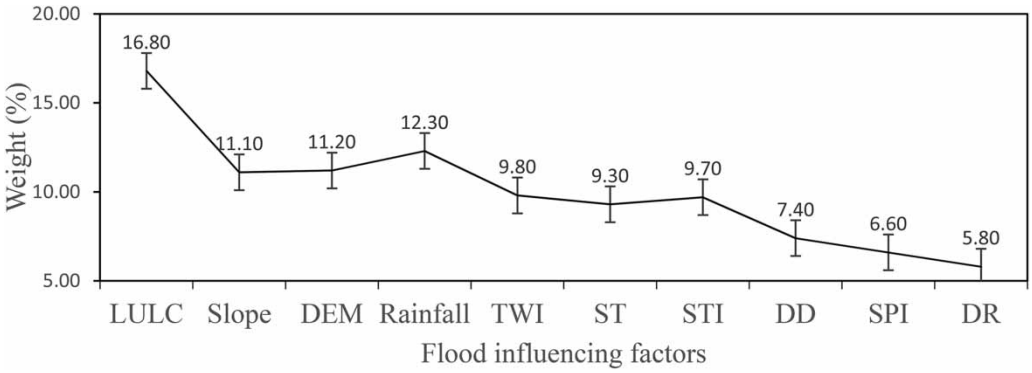

Figure 2 | Flood-influencing factors and their respective weights.

each criterion, evaluating their relative values, and determining an overall status of the alternative's affordability, value, and danger. By giving suitable weights to numerous input criteria, the multi-criteria decision-making technique has been widely used to address multifaceted difficulties (Odu 2019). In this study, the AHP was used to compute the weights of all input features for flood risk mapping. The pairwise comparison matrix comes in handy when determining weight values. After that, each pairwise comparison matrix element was divided by the total of each column to create the normalized matrix. The average value of each row was used to create the final weight value of the equivalent parameter. The comparison matrix A for any problem can be represented by the following decision matrix (Jabbar *et al.* 2019) (Equation (9)):

Step 1.

A. Construct a pairwise comparison matrix ($n \times n$) for criteria with respect to objective by using Saaty's 1–9 scale of pairwise comparisons as shown in Table 1. In other words, it is used to compare each criterion with each other criterion, one-by-one.
B. For each comparison, we will decide which of the two criteria is most important, and then assign a score to show how much more important it is.
C. Compute each element of the comparison matrix by its column total and calculate the priority vector by finding the row averages.
D. Weighted sum matrix is found by multiplying the pairwise comparison matrix and priority vector.
E. Dividing all the elements of the weighted sum matrix by their respective priority vector elements.
F. Compute the average of this value to obtain $\lambda_{\max}$.
G. Find the consistency index, CI, as follows (Equation (4)):

$$\mathrm{CI} = \frac{\lambda_{\max} - n}{n - 1} \tag{4}$$

where n is the matrix size.

Table 1 | Saaty's 1–9 scale of pairwise comparisons (Edamo *et al.* 2022a, 2022b, 2022c)

Intensity of importance	Definition	Explanation
1	Equal importance	Two activities contribute equally to the objective
2	Weak or slight	
3	Moderate importance	Experience and judgement slightly favor one activity over the other
4	Moderate plus	
5	Strong importance	Experience and judgment strongly favor one activity over another
6	Strong plus	
7	Very strong	An activity is favored very strongly over another
8	Very, very strong	
9	Extreme importance	The evidence favoring one activity over another is of the highest possible order of affirmation

H. Calculate the consistency ratio, CR, as follows (Equation (5)):

$$\mathrm{CR} = \frac{\mathrm{CI}}{\mathrm{RI}} \tag{5}$$

I. Judgment consistency can be checked by taking the consistency ratio (CR) of the CI with the appropriate value as shown in Table 2. The CR is acceptable, if it does not exceed 0.10. If it is more, the judgment matrix is inconsistent. To obtain a consistent matrix, judgments should be reviewed and improved.

Step 2:

Construct a decision matrix ($m \times n$) that includes m personnel and n criteria. Calculate the normalized decision matrix for positive criteria (Equations (6) and (7)):

$$n_{ij} = \frac{r_{ij}}{r_j^*} \; i = 1, \ldots m, \; j = 1, \ldots n \tag{6}$$

$$n_{ij} = \frac{r_j^{\min}}{r_{ij}} \; i = 1, \ldots m, \; j = 1, \ldots n \tag{7}$$

r_j^* indicates maximum number of r in the column of j

Step 3:

Evaluate each alternative, A_i by the following formula (Equation (8)):

$$A_i = \sum w_j \cdot x_{ij} \tag{8}$$

where x_{ij} is the score of the ith alternative with respect to the jth criteria, w_j is the weighted criteria

$$A = \begin{pmatrix} 1 & a_{12} & \cdots & a_{1n} \\ 1/a_{12} & 1 & a_{23} & a_{2n} \\ \cdots & 1/a_{23} & \cdots & \cdots \\ 1/a_{1n} & 1/a_{2n} & \cdots & 1 \end{pmatrix} \tag{9}$$

where a_{ij}; $i, j = 1, 2, \ldots\ldots, n$ is the element of row i and column j of the matrix and equal to the number of alternatives. Decision-makers trade-off the importance of elements, one to another, in a pairwise fashion. The judgments are entered into a pairwise comparison matrix (table of rows and columns). Each position in the matrix contains a number that is a ratio of how important the row element is to the column element. In the AHP, column is the vertical arrangement of elements and the horizontal arrangement of the same elements are called row.

Table 2 | Average random consistency (RI) (Edamo *et al.* 2022a, 2022b, 2022c)

Size of matrix	Random consistency
1	0
2	0
3	0.58
4	0.9
5	1.12
6	1.24
7	1.32
8	1.41
9	1.45
10	1.49

The Eigen vector was calculated for each row using the following equation:

$$Eg_i = \sqrt[n]{a_{11}xa_{12}xa_{13}x\ldots a_{1n}} \tag{10}$$

where Eg_i is the Eigen vector for the row i; n is the number of elements in row i.

The priority vector ($\Pr_i$) was identified by normalizing the Eigen values to 1 using the following equation:

$$\Pr_i = \frac{Eg_i}{\left(\sum_{k=1}^{n} Eg_k\right)} \tag{11}$$

In pairwise comparison matrix A, the element a_{ij} of the matrix is identified as the relative importance of the alternatives ith and jth with consideration to criterion A as shown in Equation (9) where a_{ji} is the reciprocal values of a_{ij}.

Saaty (Wind & Saaty 1980) proved consistent reciprocal matrix, the largest Eigen value is equal to the size of comparison matrix, $\lambda_{\max} = n$. Then, Saaty gave a measure of consistency, called CI as deviation or degree of consistency.

Knowing the CI, the next question is how do we use this index? Wind & Saaty (1980) proposed that we use this index by comparing it with the appropriate one. The appropriate CI is called Random Consistency Index (RI). The Random Index (RI) is the average of CI values of various sizes of comparison matrices (Edamo *et al.* 2022a, 2022b, 2022c). The RI represents the random index that refers to the consistency of the pairwise comparison matrix which is randomly generated. It is obtained as the average of the random consistency index, which was computed by Wind & Saaty (1980) using a sample of 500 matrixes randomly generated. Wind and Saaty randomly generated reciprocal matrix using scale 1/9, 1/8, …, 1, …, 8, 9 and get the random consistency index to see if it is about 10% or less. Then, they proposed what is called CR, which is a comparison between CI and Random Consistency Index (RI).

The CR was computed to determine the degree of consistency between the weight values of distinct parameters throughout the weight value determination step. A CR value of less than or equal to 0.1 indicates that the pairwise comparison matrixes are stable, but values more than 0.1 indicate that the matrixes should be reconsidered.

2.4.1. Weighted overlay

In flood susceptibility mapping, several flood-influencing factors are critical and multiplied by the associated weight value (Parsian *et al.* 2021) to prepare the flood susceptibility map. Weighted overlay was utilized to evaluate many factors of varying relevance in order to make a final decision. It helps to demonstrate how raster analysis and raster arithmetic can be utilized to solve spatial challenges (Aksha *et al.* 2020).

3. RESULTS AND DISCUSSION

Researchers from all over the world have recently stressed the relevance of decision-making approaches based on GIS techniques in flood-prone zonation, which is both cost- and time-effective (Abdel Hamid *et al.* 2020). The probable flood susceptibility map of the Bilate catchment is developed using the AHP, which takes into account 18 topographic and climatic parameters. All of these elements, as well as the outcomes, are covered in the following.

3.1. Flood drivers

There were 18 flood-influencing factors discovered in this research. The identified factors are the most deriving agents of flood hazard in the Bilate catchment. All the flood-causing factors have no equal impact (Bui *et al.* 2019).

3.1.1. Elevation

Elevations in the study area were classified into five flood susceptibility classes: very high (2,701–3,324 m), high (2,201–2,700 m), medium (1,901–2,200 m), low (1,601–1,900 m), and very low (1,174–11,600 m) (Figure 3(a)). Table 3 indicated that the lowest elevation (1,174–1,600 m) covers an area of 1,609.4 km^2 (28.6%) and the highest elevation (2,701–3,324) covered an area of 208.8 km^2 (3.6%). Flood affected the dwellers living near to the outlet of the Bilate catchment. The lowest elevation class had a very high flood susceptibility classification, while the

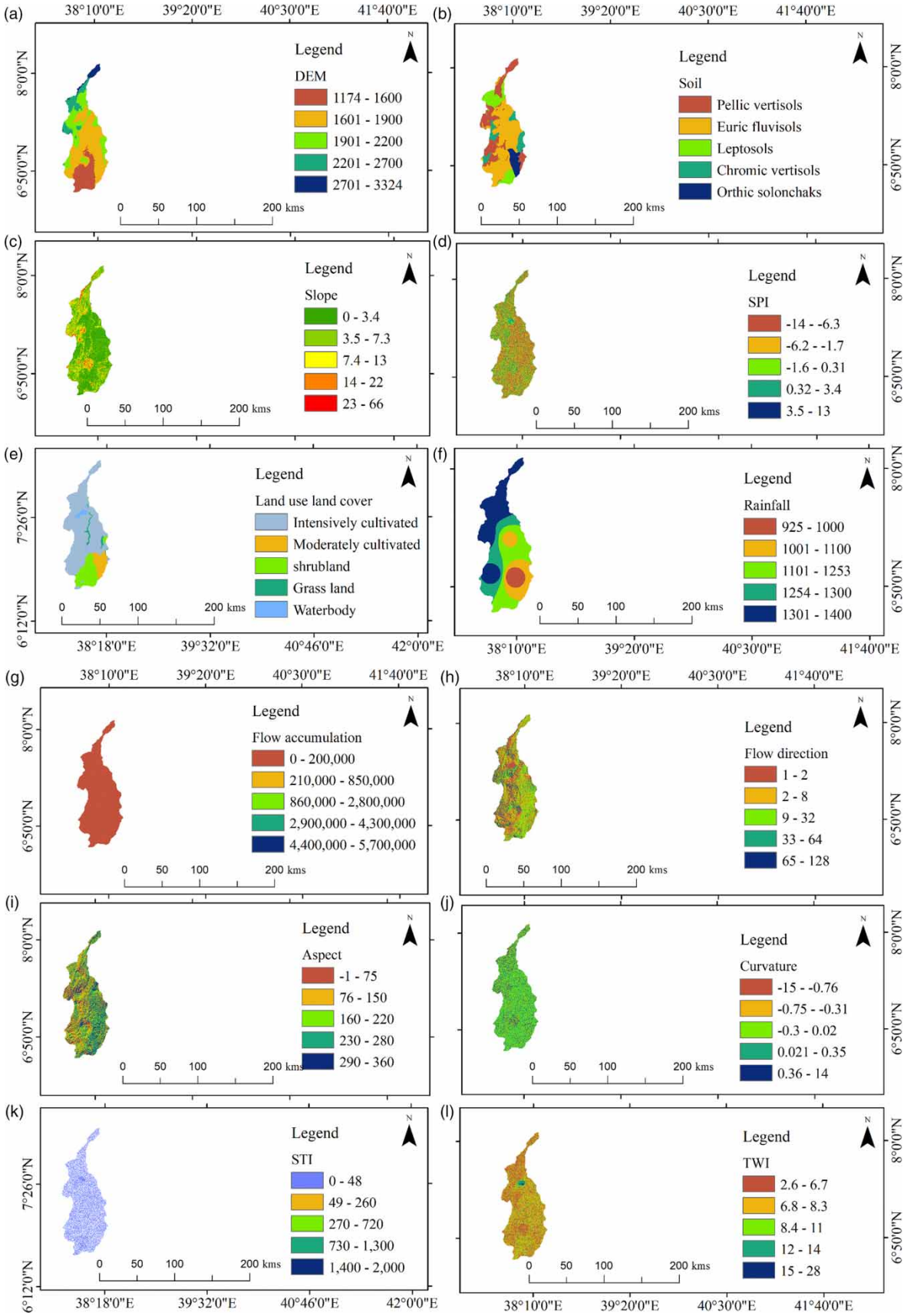

Figure 3 | Flood-influencing factors: (a) DEM, (b) soil type, (c) slope, (d) SPI, (e) LULC, (f) rainfall, (g) flow accumulation, (h) flow direction, (i) aspect, (j) curvature, (k) STI, (l) TWI, (m) geology, (n) geomorphology, (o) population density, (p) DD, (q) TRI, and (r) the distance from river. *(continued.)*.

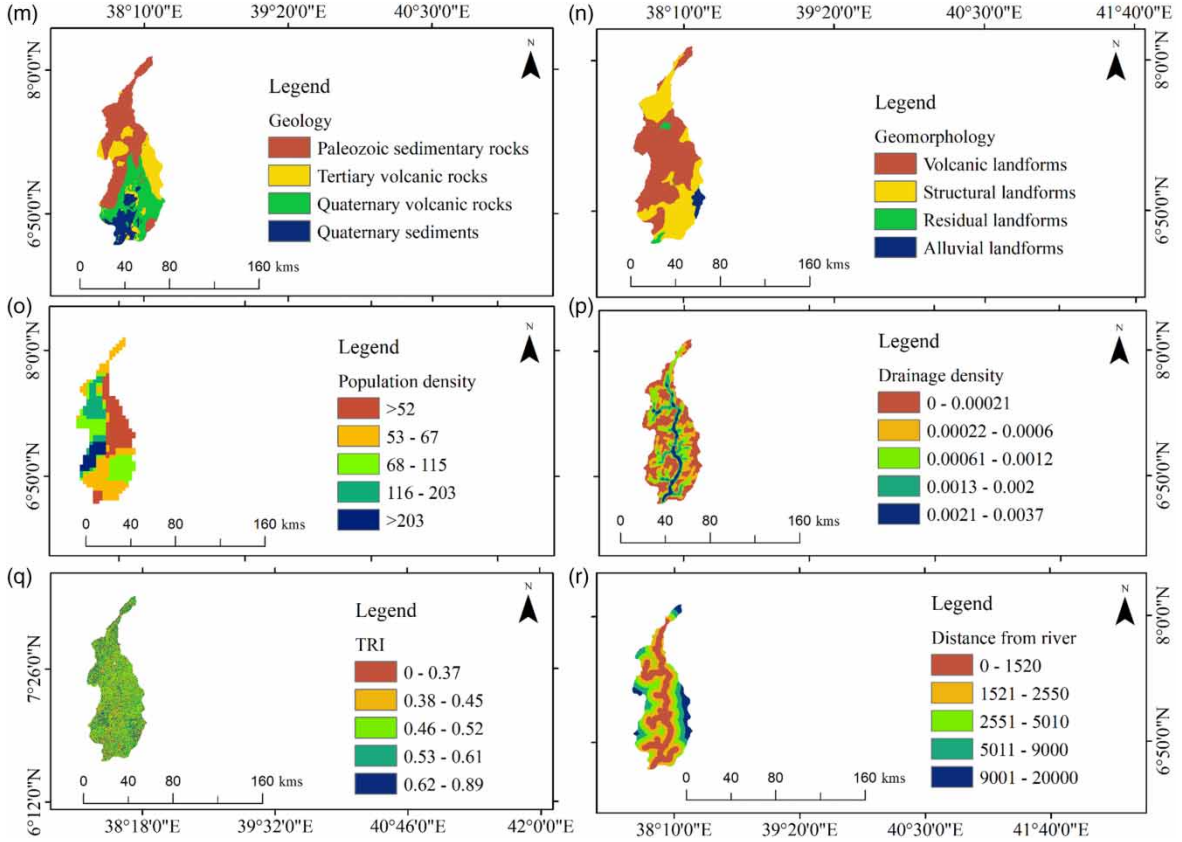

Figure 3 | Continued.

Table 3 | The elevation factor of the Bilate catchment

Elevation (m)	Area (km^2)	Area (%)
1,174–1,600	1,609.4	28.6
1,601–1,900	2,064.8	36.7
1,901–2,200	647.5	11.5
2,201–2,700	1,094.5	19.5
2,701–3,324	208.8	3.6
Total	5,625	100

highest elevation class had a very low flood susceptibility classification. Previous studies neglected flood susceptibility mapping in the Bilate catchment (Nannawo *et al.* 2021; Orke & Li 2021; Edamo *et al.* 2022a, 2022b, 2022c). This study plays a great role in flood risk management.

3.1.2. Soil type

The soil groups of the study area are reclassified into the following five classes: Pellic vertisols, Euric fluvisols, Leptosols, Chromic vertisols, and Orthic solonchaks (Figure 3(b)). The Leptosols and Pellic vertisols are the dominant soil type in the Bilate catchment (Table 4) and cover an area of 2,123.3 km^2 (37.7%) and 1,830.7 km^2 (32.5%), respectively. The nature of the soil in a given area influences the flood levels and possibly regulates the infiltration capacity. Leptosols have a high infiltration rate and a high degree of a flood risk.

3.1.3. Slope

The slope of the Bilate catchment was classified into five slope classes: very high slope, high slope, medium slope, low slope, and very low slope. The slope of the Bilate catchment fluctuates from 0° to 66° (Figure 3(c)). It is

Table 4 | The soil type factor of the Bilate catchment

Soil types	Area (km^2)	Area (%)
Pellic vertisols	1,830.7	32.5
Euric fluvisols	265.9	4.7
Leptosols	2,123.3	37.7
Chromic vertisols	1,077.2	19.2
Orthic solonchaks	328	5.8
Total	5,625	100

observed that the slope range (0°–3.4°) covered the largest land 2,133.2 km^2 (37.9%) (Table 5). In hydrological research, slope is a significant topographic factor in controlling the flow of surface water (Tehrany *et al.* 2013). According to Zaharia *et al.* (2019), regions with slopes greater than 15° have less water accumulation. The obtained average slope causing flood in the catchment was 5.13°.

3.1.4. Stream Power Index

The SPI values for the Bilate catchment in Figure 3(d) range from −14 to 13. The SPI of the study area is divided into five levels according to the flood susceptibility, very high (−14 to (−6.3)), high (−6.2 to (−1.7)), medium (−1.6 to 0.31), low (0.32–0.34), and very low (3.5–13), respectively (Figure 3(d)). The area with a high SPI implies the area of high exposure to the erosive power of runoff and soil erosion (Table 6). The increasing value of the SPI resulted from a high slope and high flow rate of water in a given area. As a result, the amount of water contributed to the upward slope and increased water flow rate, resulting in a high rate of the SPI value and sediment deposition downstream of the catchment. That is why, the downstream of the watershed had a very high flood susceptibility in comparison to the upstream of the watershed. The SPI determines the capacity of a stream to carry sediment. As a result, the SPI values in most flood-affected regions are the lowest (−14 to (−6.3)).

Table 5 | The slope factor of the Bilate catchment

Slope (°)	Area (km^2)	Area (%)
0–3.4	2,133.2	37.9
3.5–7.3	1,902.3	33.8
7.4–13	560.5	10
14–22	892.9	15.9
23–66	136.0	2.4
Total	5,625	100

Table 6 | The SPI factor of the Bilate catchment

SPI	Area (km^2)	Area (%)
−14 to (−6.3)	2,800.7	49.8
−6.2 to (−1.7)	387.9	6.9
−1.6 to 0.31	431.3	7.7
0.32–3.4	1,777.2	31.6
3.5–13	227.8	4
Total	5,625	100

3.1.5. Land use/land cover

The LULC of the Bilate catchment was grouped into five classes (Figure 3(e)). The LULC map of the Bilate catchment include 3,892.2 km^2 (69.2%) of intensively cultivated, 882.3 km^2 (15.7%) of moderately cultivated, 590.5 km^2 (10.5%) of shrub-land, 221.9 km^2 (3.7%) of grassland, and 38 km^2 (0.7%) of water body (Table 7). Land use and land cover are crucial factors in identifying areas that are at risk of flooding (Ghosh & Kar 2018).

3.1.6. Rainfall

Figure 3(f) shows that the upstream of the catchment receives the high annual rainfall, whereas the downstream of the watershed receives the low annual rainfall. Even though the upstream rainfall amount is slightly higher than that of the downstream rainfall of the catchment, the downstream areas have relatively flat topography and flat slope, which indicate it is highly vulnerable to flood hazard. According to Radwan *et al.* (2019), flood hazard increases with an increase in precipitation. Table 8 shows the various average rainfall classes, which are very low (925–1,000 mm), low (1,001–1,100 mm), medium (1,101–1,253 mm), high (1,254–1,300 mm) and very high (1,301–1,400 mm) rainfall, respectively.

3.1.7. Flow accumulation

Flow accumulation is among the most important criteria in determining flood hazard regions (Kazakis *et al.* 2015). Flooding occurs in regions with a lot of water (Tehrany *et al.* 2015). Flow accumulation is often lower for the lower classes of rivers in the upstream. In the downstream of the watershed, many tributaries join the main channel, which increases the flow accumulation and the flood risk. Therefore, high flow accumulation can be found in the downstream region of the study area. An increase in flow accumulation exacerbates the occurrence of flood (Abdel Hamid *et al.* 2020) (Figure 3 (g)). Flow accumulation is often lower for the lower classes of rivers in the upstream. In the downstream of the catchment, many tributaries join the main channel, which increases the flow accumulation and the flood risk. Therefore, high flow accumulation can be found in the downstream region of the study area. The flow accumulation and the area coverage of the Bilate catchment are given in Table 9.

3.1.8. Flow direction

One of the fundamental advantage of the GIS is its ability to differentiate the flow direction of each raster pixel. The flow direction in the map of the Bilate catchment is presented in Figure 3 (h). The flow direction is a grid whose value shows how each cell flows with respect to its closest downward slope neighbour (Sanyal 2004). Flow direction was divided into the following five categories: 1–2, 2–8, 9–32, 33–64, and 65–128. Low flow

Table 7 | The LULC factor of the Bilate catchment

LULC	Area (km^2)	Area (%)
Intensively cultivated	3,892.2	69.2
Moderately cultivated	882.3	15.7
Shrub-land	590.5	10.5
Grassland	221.9	3.7
Water body	38	0.7
Total	5,625	100

Table 8 | The rainfall factor of the Bilate catchment

Rainfall (mm)	Area (km^2)	Area (%)
925–1,000	200.9	3.6
1,001–1,100	902.3	16
1,101–1,253	560.5	10
1,254–1,300	3,925.2	69.8
1,301–1,400	36.0	0.6
Total	5,625	100

Table 9 | The flow accumulation factor of the Bilate catchment

Flow accumulation	Area (km²)	Area (%)
0–200,000	3,869.2	68.8
210,000–850,000	265.9	4.7
860,000–2,800,000	431.3	7.7
2,900,000–4,300,000	227.8	4
4,400,000–5,700,000	830.7	14.7
Total	5,625	100

directions imply a high probability of flooding, whereas high flow directions show a low probability of flooding (Table 10). The flow direction ranged (1–2) covered the largest area (48.2%) of the catchment.

3.1.9. Aspect

Index of aspect is derived from the elevation that defines the pixel directions per unit degree, allowing for more precise flood risk mapping judgments. It is often referred to as the horizontal direction of the mountain facing, and it determines the local climatological conditions. Aspect of the catchment was ranged from −1 to 360 (Figure 3(i)). It was divided into the following five categories: –1 to 75, 76–150, 160–220, 230–280, and 290–360 (Table 11).

3.1.10. Curvature

The curvature map of the study area is presented in Figure 3(j). Table 12 implied that the curvature is classified into the following five classes: −15 to (−0.76), −0.75 to (−0.31), −0.3 to (−0.02), 0.021–0.35, and 0.36–14, respectively. A positive value of curvature represents a convex surface, zero a flat surface, and a negative value a concave surface (Das 2019). Hudson & Kessel (2000) observed that curvature between 1.0 and 2.0 had a greater probability of flooding. Hence, the probability of flood is very high between the curvature from 1.6 to 22 and very low between −19 and (−2.2), respectively. Similarly, curvature is also an important factor and represents the morphology of the topography (Das 2018).

Table 10 | The flow direction factor of the Bilate catchment

Flow direction	Area (km²)	Area (%)
1–2	2,734.7	48.2
2–8	1,696	30.2
9–32	664.3	11.8
33–64	301.3	5.4
65–128	228.1	4.1
Total	5,625	100

Table 11 | The aspect factor of the Bilate catchment

Aspect	Area (km²)	Area (%)
–1 to 75	1,431.3	25.4
76–150	830.7	14.8
160–220	265.9	4.7
230–280	2,077.2	36.9
290–360	1,019.5	18.1
Total	5,625	100

Table 12 | The curvature factor of the Bilate catchment

Curvature	Area (km^2)	Area (%)
−15 to (−0.76)	1,609.4	28.6
−0.75 to (−0.31)	2,064.8	36.7
−0.3 to (−0.02)	647.5	11.5
0.021–0.35	909.5	16.2
0.36–14	394.5	7
Total	5,625	100

3.1.11. Sediment Transport Index

The STI of the Bilate catchment ranges from 0 to 140 (Figure 3 (k)). It was classified as very high (0–48), high (49–260), medium (270–720), low (730–1,300), and very low (1,400–2,000) (Table 13). Due to silt deposition, the carrying capacity of stream channels in this catchment will be greatly diminished, and it could cause flooding. The highest STI covers an area of 2,666.3 (47.4%), and the lowest STI covers an area of 1,102.4 (19.6%). STI is sediment transport caused by flowing water (Shafapour Tehrany *et al.* 2019). The higher STI indicates the area with more sediment transport, and the lower STI indicates less sediment transport. The chance of flooding will be high in areas with low STI values (0–48) because these are the depositional zones.

3.1.12. Topographic Wetness Index

Flood is more likely in areas with a bigger TWI (Mojaddadi *et al.* 2017). Lower TWI zones, on the other hand, are less vulnerable to flooding (Figure 3 (l)). The higher value was assigned for the higher TWI and the lower value was assigned for the lower TWI, respectively. As a result, the downstream of the Bilate catchment has the highest TWI and has a larger probability of flooding than the upstream of the catchment, which has the lowest TWI and has a lower probability of flooding. The lowest TWI covers an area of 265.9 km^2 (4.7%) in class between 6.8 and 8.3 whereas the highest TWI cover an area of 2,077.2 km^2 (36.9%) in class between 12 and 14, respectively (Table 14).

Table 13 | The STI factor of the Bilate catchment

STI	Area (km^2)	Area (%)
0–48	2,666.3	47.4
49–260	72.9	1.3
270–720	943.4	16.8
730–1,300	840.1	14.9
1,400–2,000	1,102.4	19.6
Total	5,625	100

Table 14 | The TWI factor of the Bilate catchment

TWI (TWI)	Area (km^2)	Area (%)
2.6–6.7	1,830.7	32.5
6.8–8.3	265.9	4.7
8.4–11	492	8.7
12–14	2,077.2	36.9
15–28	959.2	17.1
Total	5,625	100

Table 15 | The surficial geology factor of the Bilate catchment

Surficial geology	Area (km^2)	Area (%)
Paleozoic sedimentary rocks	1,900.7	33.8
Tertiary volcanic rocks	455.9	8.1
Quaternary volcanic rocks	401.3	7.1
Quaternary sedimentary rocks	2,867.1	51
Total	5,625	100

3.1.13. Surficial geology

The lithological properties of an area influence porosity and permeability. Such factors/properties of a rock can influence flood intensity. The geology affects the catchment runoff by formation of different permeable and impermeable rocks. The Bilate catchment is separated into four primary divisions geologically such as paleozoic sedimentary rocks, tertiary volcanic rocks, quaternary volcanic rocks, and quaternary sedimentary rocks (Figure 3 (m)). The area coverage of the surficial geology of the Bilate catchment is presented in Table 15.

3.1.14. Geomorphology

Geomorphology is the driving agent of flooding. The landforms of the Bilate catchment are presented in Figure 3(n). Volcanic landforms are sensitive to flooding which covers 47.1% of the study area. The area coverage of the geomorphology of the Bilate catchment is presented in Table 16. The alluvial landforms covered 13.1% of the catchment.

3.1.15. Population density

The population is densely distributed in the Bilate catchment (Figure 3(o)). The population density layer was further reclassified into five density classes as very high, high, medium, low and very low population densities (Table 17). The reclassified population density of the study area are <52, 53–67, 68–115, 116–203, and >200, respectively. Therefore, the lowest population density <52 covered an area of 137.1 per square kilometres (2.4%) (Table 17). Floods can occur often in highly populated places due to a lack of appropriate drainage systems (Ogato *et al.* 2020a). Population density was reclassified based on the assumption that the denser the population, the more prone it is to floods (Ogato *et al.* 2020a).

Table 16 | The geomorphology factor of the Bilate catchment

Geomorphology	Area (km^2)	Area (%)
Volcanic landforms	2,644.33	47.1
Structural landforms	1,245	22.1
Residual landforms	997.0	17.7
Alluvial landforms	738.7	13.1
Total	5,625	100

Table 17 | The population density factor of the Bilate catchment

Population density (person/km^2)	Area (km^2)	Area (%)
<52	137.1	2.4
53–67	3,213.7	57.1
68–115	1,210.5	21.5
116–203	906.5	16.1
>203	157	2.8
Total	5,625	100

3.1.16. Drainage density

According to the classification shown in Figure 3(p), a higher DD area was very heavily affected by flood and ranked in class five, whereas a lower DD area was very lightly affected by flood and ranked in class one. The DD has a big influence on flood peaks. The control related to the length of the stream network and hillslope routes has the most substantial effects. DD considerably influences the concentration-time and thus the peak flow magnitude because the river network has a larger flow velocity. As a result, as DD increases, flood peaks rise as well. Furthermore, a long concentration-time means there are more chances for water to permeate. If the DD is high, it creates a high runoff rate and causes a higher flood risk (Shekhar & Pandey 2015). The density of drainage is divided into the following five categories: 0–0.00021, 0.00022–0.0006, 0.00061–0.0012, 0.0013–0.002, and 0.0021–0.0037 (Table 18).

3.1.17. Terrain Ruggedness Index

The TRI is a secondary geo-morphometric measure for describing and quantifying local relief. The TRI influences the river flooding; however it was not considered in the flood susceptibility mapping in different studies (Riley *et al.* 1999). The TRI value of the Bilate catchment was presented in Figure 3(q). It provides new information on terrain morphology and is suggested for usage, particularly in characterizing flood damage sections.

The topographic ruggedness index measures the uniformity in the terrain distribution of altitude (Riley *et al.* 1999). This technique is quite useful for determining whether a region is flat or rugged (Das 2021). The regions with a low TRI rating have a greater risk of flooding because of their flat nature. As a result, very low TRI values can be found in flood plains. The TRI of the Bilate catchment is classified into five classes; as very high (0–0.37), high (0.38–0.45), medium (0.46–0.52), low (0.53–0.61) and very low (0.62–0.89), respectively (Table 19).

3.1.18. Distance from the river

It plays a key role in identifying flood sensitive regions. As the distance from the river is far from the likelihood of flooding is less. The distance range in the Bilate catchment is found between 0 and 19,000 m (Figure 3(r)). Further development of this study's findings may focus on the inclusion of a greater number of potential conditioning factors. An area close to the river hence has more flood than areas farther away from river and vice versa. The majority of Bilate people live near the river bank, making them subject to flooding. The distances were classified into five classes as 0–1,520 m, 1,521–2,550 m, 2,551–5,010m, 5,011–9,000 m and 9,001–20,000 m, respectively (Table 20). The nearest distance to the watershed (0–1,520 m) covered an area of 834.7 km^2 (14.8%) whereas

Table 18 | The DD factor of the Bilate catchment

DD	Area (km^2)	Area (%)
0–0.00021	804.6	14.3
0.00022–0.0006	2,470.7	43.9
0.00061–0.0012	2,200.7	39.1
0.0013–0.002	100.1	1.8
0.0021–0.0037	49.1	0.9
Total	5,625	100

Table 19 | The TRI factor of the Bilate catchment

TRI	Area (km^2)	Area (%)
0–0.37	891.8	15.9
0.38–0.45	742.1	13.2
0.46–0.52	1,790.9	31.8
0.53–0.61	1,836.6	32.7
0.62–0.89	362.6	6.5
Total	5,625	100

Table 20 | Distance from the river factor of the Bilate catchment

Distance from the river (m)	Area (km^2)	Area (%)
0–1,520	834.7	14.8
1,521–2,550	2,270.7	40.4
2,551–5,010	2,219.7	39.5
5,011–9,000	205.3	3.6
9,001–20,000	94.8	1.7
Total	5,625	100

the farthest distance to the watershed (9,001–20,000 m) cover an area of 94.8 km^2 (1.7%). Hence, the largest area of the watershed covered an area of 2,270.7 km^2 (40.4%) which is in between 1,521 and 2,550 m (Table 20).

3.2. Weight of flood drivers in the Bilate catchment

The weight of the factors were obtained and overlay process was accomplished in ArcGIS 10.3 environment. The CR, the Random Consistency Index (RI), and the CI were calculated as 0.061, 1.49 and 0.078, respectively.

The use of multiple flood conditioning factors is useful to determine the capacity of effective flood danger management in flood-prone catchments since there is variation in flood causing from catchment to catchment and region to region. Rimba *et al.* (2017) used six flood-influencing factors (LULC, slope, soil, DD, and rainfall) and found that rainfall was the most flood causing factor in Okazaki City, Japan. However, the number of variables was limited, making the outcome highly doubted.

A pairwise comparison matrix was constructed to determine the proper weight, indicating the contribution of each component that influences flood (Table 21). The matrix normalization method is used in this study to compute the importance of the various flood-related parameters.

3.3. Flood susceptibility mapping

The degree of flood susceptibility is divided into the following five categories: very low, low, moderate, high and very high, with 9.3, 32.6, 41.2, 10.8, and 6.1% of the entire Bilate catchment, respectively (Figure 4). In order to avoid future flood circumstances, authorities should pay special attention to regions classified as high flood zones. Using geospatial approaches (Das 2018) attempted to identify likely high flood risk zones using an AHP. The advantages of the multi-criteria approach was to prepare the flood map for the whole catchment. It is a challenging task to complete flood susceptibility mapping in a catchment using hydrodynamic models (Di Baldassarre *et al.* 2010; Tehrany *et al.* 2019). AHP helped to overcome the shortcomings of hydraulic/hydrologic models. The map developed in this study will play a significant role in flood risk management. It will also help as the source of information for further researches. The identified flood causing factors can be used in different parts of the world for flood-related investigations.

Table 21 | Standardization matrix

Factors	Slope	DEM	ST	Rainfall	TWI	DD	LULC	DR	SPI	STI	Weight
Slope	0.123	0.117	0.101	0.147	0.199	0.290	0.126	0.171	0.102	0.102	0.111
DEM	0.123	0.117	0.101	0.147	0.133	0.174	0.126	0.171	0.102	0.102	0.112
ST	0.123	0.117	0.101	0.147	0.199	0.058	0.063	0.057	0.102	0.102	0.093
Rainfall	0.123	0.117	0.101	0.147	0.199	0.116	0.252	0.171	0.102	0.102	0.13
TWI	0.041	0.059	0.034	0.049	0.066	0.058	0.042	0.171	0.102	0.102	0.098
DD	0.025	0.039	0.101	0.073	0.066	0.058	0.025	0.057	0.102	0.102	0.08
LULC	0.123	0.117	0.202	0.073	0.199	0.290	0.126	0.171	0.102	0.102	0.168
DR	0.041	0.039	0.101	0.049	0.022	0.058	0.042	0.057	0.102	0.102	0.052
SPI	0.123	0.117	0.101	0.147	0.066	0.058	0.126	0.057	0.102	0.102	0.064
STI	0.123	0.117	0.101	0.147	0.066	0.058	0.126	0.057	0.102	0.102	0.09

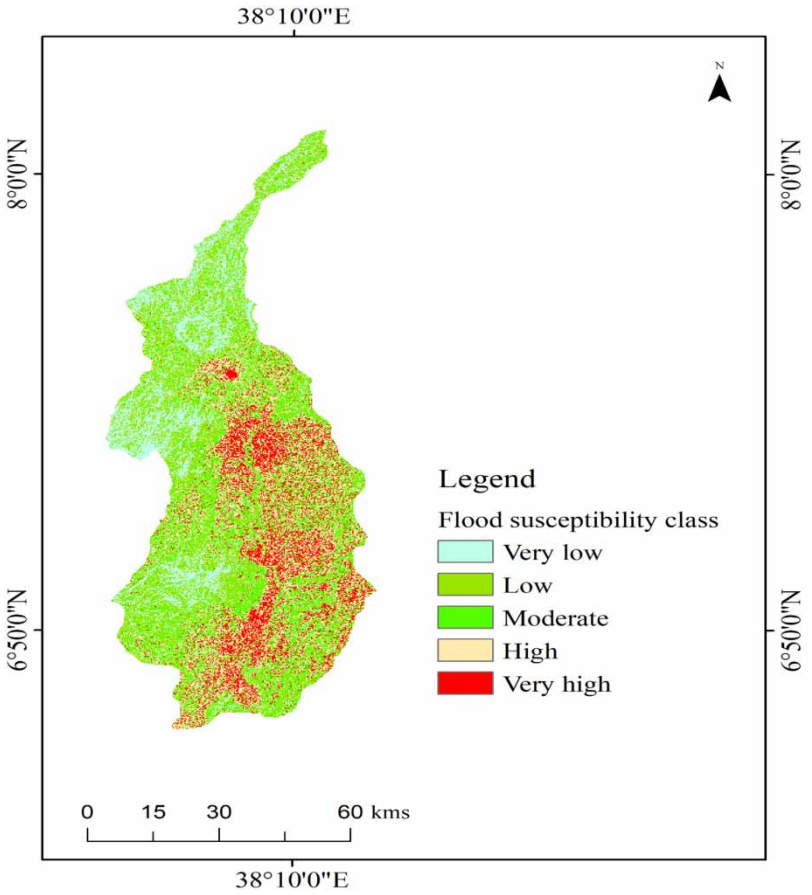

Figure 4 | Flood susceptibility map.

4. CONCLUSIONS

Flooding is a destructive incident that can occur nearly anywhere along a river's route, especially downstream. Using remote sensing and GIS methods, flood conditioning factors were identified to define flood-prone zones in the Bilate catchment and identify more vulnerable locations. To combine the decision measures in this study, the multi-criteria method was used. LULC (16.8%) is the most flood-influencing factor in the catchment. The whole Bilate catchment suffered flood susceptibility ranging from very high to very low. The very high flood susceptibility covered approximately (6.1%) of the total land area. The flood susceptibility map provided in this study will be a useful resource for construction managers, decision-makers, administrators, financiers, and administrative authorities involved in organizing response and emergency services during floods. In addition, it will play a significant role in assessing flood risks not just in the Bilate catchment but also in other flood-prone watersheds prone to flood events across the nation. As a result, it is advised that more elements should be employed as an effective technique for possible flood mapping studies to increase the successful control of flood damage.

FUNDING STATEMENT

No fund was provided from any source.

DATA AVAILABILITY STATEMENT

All relevant data are included in the paper or its Supplementary Information.

CONFLICT OF INTEREST

The authors declare there is no conflict.

REFERENCES

Abdel Hamid, H. T., Wenlong, W. & Qiaomin, L. 2020 Environmental sensitivity of flash flood hazard using geospatial techniques. *Global Journal of Environmental Science and Management* **6** (1), 31–46. https://doi.org/10.22034/gjesm.2020.01.03.

Ajin, R. S., Krishnamurthy, R. R., Jayaprakash, M. & Vinod, P. G. 2013 Flood hazard assessment of Vamanapuram River Basin, Kerala, India: an approach using remote sensing and GIS techniques. *Advances in Applied Science Research* **4** (3), 263–274.

Aksha, S. K., Resler, L. M., Juran, L. & Carstensen, L. W. 2020 A geospatial analysis of multi-hazard risk in Dharan, Nepal. *Geomatics, Natural Hazards and Risk* **11** (1), 88–111.

Alaska Satellite Facility (ASF) source. Available from: https://asf.alaska.edu/.

Ali, A. b. M. 2018 *Flood Inundation Modeling and Hazard Mapping Under Uncertainty in the Sungai Johor Basin, Malaysia*. https://doi.org/10.1201/9780429469015.

Antzoulatos, G., Kouloglou, I. O., Bakratsas, M., Moumtzidou, A., Gialampoukidis, I., Karakostas, A., Lombardo, F., Fiorin, R., Norbiato, D., Ferri, M., Symeonidis, A., Vrochidis, S. & Kompatsiaris, I. 2022 Flood hazard and risk mapping by applying an explainable machine learning framework using satellite imagery and GIS data. *Sustainability (Switzerland)* **14** (6). https://doi.org/10.3390/su14063251.

Ayele, M. A., Lohani, T. K., Mirani, K. B., Edamo, M. L. & Ayalew, A. T. 2022 Simulating sediment yield by SWAT and optimizing the parameters using SUFI-2 in Bilate river of Lake Abaya in Ethiopia. *World Journal of Engineering* https://doi.org/10.1108/wje-07-2021-0449.

Bibi, T., Nawaz, F., Abdul Rahman, A. & Latif, A. 2019 Flood hazard assessment using participatory approach and weighted overlay methods. *International Archives of the Photogrammetry, Remote Sensing and Spatial Information Sciences – ISPRS Archives* **42** (4/W16), 153–160. https://doi.org/10.5194/isprs-archives-XLII-4-W16-153-2019.

Bui, D. T., Ngo, P. T. T., Pham, T. D., Jaafari, A., Minh, N. Q., Hoa, P. V. & Samui, P. 2019 A novel hybrid approach based on a swarm intelligence optimized extreme learning machine for flash flood susceptibility mapping. *Catena* **179** (October 2018), 184–196. https://doi.org/10.1016/j.catena.2019.04.009.

Cea, L. & Costabile, P. 2022 Flood risk in urban areas: modelling, management and adaptation to climate change. A review. *Hydrology* **9** (3), 50. https://doi.org/10.3390/hydrology9030050.

Chen, J., Li, Q., Wang, H. & Deng, M. 2020 A machine learning ensemble approach based on random forest and radial basis function neural network for risk evaluation of regional flood disaster: a case study of the Yangtze river delta, China. *International Journal of Environmental Research and Public Health* **17** (1), 1–21. https://doi.org/10.3390/ijerph17010049.

Cinelli, M., Coles, S. R. & Kirwan, K. 2014 Analysis of the potentials of multi criteria decision analysis methods to conduct sustainability assessment. *Ecological Indicators* **46**, 138–148. https://doi.org/10.1016/j.ecolind.2014.06.011.

Costache, R. 2019 Flood susceptibility assessment by using bivariate statistics and machine learning models – a useful tool for flood risk management. *Water Resources Management* **33** (9), 3239–3256. https://doi.org/10.1007/s11269-019-02301-z.

Das, S. 2018 Geographic information system and AHP-based flood hazard zonation of Vaitarna basin, Maharashtra, India. *Arabian Journal of Geosciences* **11** (19). https://doi.org/10.1007/s12517-018-3933-4

Das, S. 2019 Geospatial mapping of flood susceptibility and hydro-geomorphic response to the floods in Ulhas basin, India. *Remote Sensing Applications: Society and Environment* **14** (January), 60–74. https://doi.org/10.1016/j.rsase.2019.02.006.

Das, S. 2021 Hydro-geomorphic characteristics of the Indian (Peninsular) catchments: based on morphometric correlation with hydro-sedimentary data. *Advances in Space Research* **67** (8), 2382–2397. https://doi.org/10.1016/j.asr.2021.01.043.

Das, S. & Pardeshi, S. D. 2018 Comparative analysis of lineaments extracted from Cartosat, SRTM and ASTER DEM: a study based on four watersheds in Konkan region, India. *Spatial Information Research* **26** (1), 47–57. https://doi.org/10.1007/s41324-017-0155-x.

Das, S., Pardeshi, S. D., Kulkarni, P. P. & Doke, A. 2018 Extraction of lineaments from different azimuth angles using geospatial techniques: a case study of Pravara basin, Maharashtra, India. *Arabian Journal of Geosciences* **11** (8). https://doi.org/10.1007/s12517-018-3522-6.

De Risi, R., Jalayer, F., De Paola, F. & Lindley, S. 2018 Delineation of flooding risk hotspots based on digital elevation model, calculated and historical flooding extents: the case of Ouagadougou. *Stochastic Environmental Research and Risk Assessment* **32** (6), 1545–1559. https://doi.org/10.1007/s00477-017-1450-8.

Di Baldassarre, G., Schumann, G., Bates, P. D., Freer, J. E. & Beven, K. J. 2010 Cartographie de zone inondable: Un examen critique d'approches déterministe et probabiliste. *Hydrological Sciences Journal* **55** (3), 364–376. https://doi.org/10.1080/02626661003683389.

Edamo, M. L., Bushira, K. M., Ukumo, T. Y., Ayele, M. A., Alaro, M. A. & Borko, H. B. 2022a Effect of climate change on water availability in Bilate catchment, Southern Ethiopia. *Water Cycle 3 (June)*, **86-99**. https://doi.org/10.1016/j.watcyc.2022.06.001.

Edamo, M. L., Ukumo, T. Y., Lohani, T. K., Ayana, M. T., Ayele, M. A., Mada, Z. M. & Abdi, D. M. 2022b A comparative assessment of multi-criteria decision-making analysis and machine learning methods for flood susceptibility mapping and socio-economic impacts on flood risk in Abela-Abaya floodplain of Ethiopia. Environmental Challenges 9 (October). https://doi.org/10.1016/j.envc.2022.100629.

Edamo, M. L., Ukumo, T. Y., Lohani, T. K. & Mirani, K. B. 2022c Flood inundation mapping under climate change scenarios in the Boyo watershed of Southern Ethiopia. *Journal of Water and Climate Change* **13**(8), 3170–3188. https://doi.org/10.2166/wcc.2022.193.

Galavi, H., Mirzaei, M., Shui, L. T. & Valizadeh, N. 2013 Klang River-level forecasting using ARIMA and ANFIS models. *Journal – American Water Works Association* **105** (9), 81–82. https://doi.org/10.5942/jawwa.2013.105.0106.

Ghosh, A. & Kar, S. K. 2018 Application of analytical hierarchy process (AHP) for flood risk assessment: a case study in Malda district of West Bengal, India. *Natural Hazards* **94** (1), 349–368. https://doi.org/10.1007/s11069-018-3392-y.

Hosseinzadehtalaei, P., Ishadi, N. K., Tabari, H. & Willems, P. 2021 Climate change impact assessment on pluvial flooding using a distribution-based bias correction of regional climate model simulations. *Journal of Hydrology* **598** (January), 126239. https://doi.org/10.1016/j.jhydrol.2021.126239.

Hudson, P. F. & Kessel, R. H. 2000 Channel migration and meander-bend curvature in the lower Mississippi River prior to major human modification. *Geology* **28** (6), 531–534. https://doi.org/10.1130/0091-7613(2000)028 < 0531:cmambc > 2.3.co;2.

Jabbar, F. K., Grote, K. & Tucker, R. E. 2019 A novel approach for assessing watershed susceptibility using weighted overlay and analytical hierarchy process (AHP) methodology: a case study in Eagle Creek Watershed, USA. *Environmental Science and Pollution Research* **26** (31), 31981–31997. https://doi.org/10.1007/s11356-019-06355-9.

Kablan, M. K. A., Dongo, K. & Coulibaly, M. 2017 Assessment of social vulnerability to flood in urban Côte d'Ivoire using the MOVE framework. *Water (Switzerland)* **9** (4). https://doi.org/10.3390/w9040292.

Kazakis, N., Kougias, I. & Patsialis, T. 2015 Science of the total environment assessment of flood hazard areas at a regional scale using an index-based approach and analytical hierarchy process : application in Rhodope – Evros region, Greece. *Science of the Total Environment* **538**, 555–563. https://doi.org/10.1016/j.scitotenv.2015.08.055.

Kruczkiewicz, A., Bucherie, A., Ayala, F., Hultquist, C., Vergara, H., Mason, S., Bazo, J. & de Sherbinin, A. 2021 Development of a flash flood confidence index from disaster reports and geophysical susceptibility. *Remote Sensing* **13** (14). https://doi.org/10.3390/rs13142764.

Liu, J., Xiong, J., Cheng, W., Li, Y., Cao, Y., He, Y., Duan, Y., He, W. & Yang, G. 2021 Assessment of Flood Susceptibility Using Support Vector Machine in the Belt and Road Region. *Natural Hazards and Earth System Sciences Discussions*, *May*, 1–37.

Malik, S., Pal, S. C., Arabameri, A., Chowdhuri, I., Saha, A., Chakrabortty, R., Roy, P. & Das, B. 2021 GIS-based statistical model for the prediction of flood hazard susceptibility. In: *Environment, Development and Sustainability*, Vol. 23, Issue 11. Springer, Netherlands. https://doi.org/10.1007/s10668-021-01377-1.

Maskong, H. 2019 Flood hazard mapping using on-site surveyed flood Map, Hecras V.5 and Gis Tool: a case study of Nakhon Ratchasima Municipality, Thailand. *International Journal of GEOMATE* **16** (54), 1–8. https://doi.org/10.21660/2019.54.81342.

Mehta, D. J., Eslamian, S. & Prajapati, K. 2021 Flood modelling for a data-scare semi-arid region using 1-D hydrodynamic model: a case study of Navsari Region. *Modeling Earth Systems and Environment* 0123456789. https://doi.org/10.1007/s40808-021-01259-5.

Mirzaei, M., Yu, H., Dehghani, A., Galavi, H., Shokri, V., Karimi, S. M. & Sookhak, M. 2021 A novel stacked long short-term memory approach of deep learning for streamflow simulation. *Sustainability (Switzerland)* **13** (23), 1–16. https://doi.org/10.3390/su132313384.

Mojaddadi, H., Pradhan, B., Nampak, H., Ahmad, N. & Ghazali, A. H. b. 2017 Ensemble machine-learning-based geospatial approach for flood risk assessment using multi-sensor remote-sensing data and GIS. *Geomatics, Natural Hazards and Risk* **8** (2), 1080–1102. https://doi.org/10.1080/19475705.2017.1294113.

Mundhe, N. 2019 Multi-Criteria decision making for vulnerability mapping of flood hazard: a case study of Pune City. *Journal of Geographical Studies* **2** (1), 41–52. https://doi.org/10.21523/gcj5.18020105.

Nannawo, A. S., Lohani, T. K. & Eshete, A. A. 2021 Exemplifying the effects using wetSpass model depicting the landscape modifications on long-Term surface and subsurface hydrological water balance in Bilate Basin, Ethiopia. *Advances in Civil Engineering*. https://doi.org/10.1155/2021/7283002.

Németh, B., Molnár, A., Bozóki, S., Wijaya, K., Inotai, A., Campbell, J. D. & Kaló, Z. 2019 Comparison of weighting methods used in multicriteria decision analysis frameworks in healthcare with focus on low-and middle-income countries. *Journal of Comparative Effectiveness Research* **8** (4), 195–204. https://doi.org/10.2217/cer-2018-0102.

Norman, L. M., Huth, H., Levick, L., Shea Burns, I., Phillip Guertin, D., Lara-Valencia, F. & Semmens, D. 2010 Flood hazard awareness and hydrologic modelling at Ambos Nogales, United States-Mexico border. *Journal of Flood Risk Management* **3** (2), 151–165. https://doi.org/10.1111/j.1753-318X.2010.01066.x.

Odu, G. O. 2019 Weighting methods for multi-criteria decision making technique. *Journal of Applied Sciences and Environmental Management* **23** (8), 1449. https://doi.org/10.4314/jasem.v23i8.7.

Ogato, G. S., Bantider, A., Abebe, K. & Geneletti, D. 2020a Geographic information system (GIS)-Based multicriteria analysis of flooding hazard and risk in Ambo Town and its watershed, West shoa zone, oromia regional State, Ethiopia. *Journal of Hydrology: Regional Studies* **27** (March 2019), 100659. https://doi.org/10.1016/j.ejrh.2019.100659.

Ogato, G. S., Bantider, A., Abebe, K. & Geneletti, D. 2020b Geographic information system (GIS)-Based multicriteria analysis of flooding hazard and risk in Ambo Town and its watershed, West shoa zone, oromia regional State, Ethiopia. *Journal of Hydrology: Regional Studies* **27** (December 2019), 100659. https://doi.org/10.1016/j.ejrh.2019.100659.

Orke, Y. A. & Li, M. H. 2021 Hydroclimatic variability in the bilate watershed, Ethiopia. *Climate* **9** (6). https://doi.org/10.3390/cli9060098.

Ouma, Y. O. & Tateishi, R. 2014 Urban flood vulnerability and risk mapping using integrated multi-parametric AHP and GIS: methodological overview and case study assessment. *Water (Switzerland)* **6** (6), 1515–1545. https://doi.org/10.3390/w6061515.

Ozcelik, C. & Gorokhovich, Y. 2020 An overland flood model for geographical information systems. *Water (Switzerland)* **12** (9). https://doi.org/10.3390/W12092397.

Parsian, S., Amani, M., Moghimi, A., Ghorbanian, A. & Mahdavi, S. 2021 Flood hazard mapping using fuzzy logic, analytical hierarchy process, and multi-source geospatial datasets. *Remote Sensing* **13** (23). https://doi.org/10.3390/rs13234761.

Radwan, F., Alazba, A. A. & Mossad, A. 2019 Flood risk assessment and mapping using AHP in arid and semiarid regions. *Acta Geophysica* **67** (1), 215–229. https://doi.org/10.1007/s11600-018-0233-z.

Riley, S. J., DeGloria, S. D. & Elliot, R. 1999 A terrain ruggedness index that qauntifies topographic heterogeneity. *Intermountain Journal of Sciences* **5** (1–4), 23–27.

Rimba, A., Setiawati, M., Sambah, A. & Miura, F. 2017 Physical flood vulnerability mapping applying geospatial techniques in Okazaki City, Aichi Prefecture, Japan. *Urban Science* **1** (1), 7. https://doi.org/10.3390/urbansci1010007.

Sanyal, J. 2004 Application of remote sensing in flood management with special reference to monsoon Asia: a review related papers geographic information system and remote sensing applications in flood hazards manage… Abdul-Lat eef Balogun Applicat Ion of Gis And Remo. *Natural Hazards* **33**, 283–301.

Sepehri, M., Malekinezhad, H., Jahanbakhshi, F., Ildoromi, A. R., Chezgi, J., Ghorbanzadeh, O. & Naghipour, E. 2020 Integration of interval rough AHP and fuzzy logic for assessment of flood prone areas at the regional scale. *Acta Geophysica* **68** (2), 477–493. https://doi.org/10.1007/s11600-019-00398-9.

Shafapour Tehrany, M., Kumar, L., Neamah Jebur, M. & Shabani, F. 2019 Evaluating the application of the statistical index method in flood susceptibility mapping and its comparison with frequency ratio and logistic regression methods. *Geomatics, Natural Hazards and Risk* **10** (1), 79–101. https://doi.org/10.1080/19475705.2018.1506509.

Shekhar, S. & Pandey, A. C. 2015 Delineation of groundwater potential zone in hard rock terrain of India using remote sensing, geographical information system (GIS) and analytic hierarchy process (AHP) techniques. *Geocarto International* **30** (4), 402–421. https://doi.org/10.1080/10106049.2014.894584.

Singh, S., Dhote, P. R., Thakur, P. K., Chouksey, A. & Aggarwal, S. P. 2021 Identification of flash-floods-prone river reaches in Beas river basin using GIS-based multi-criteria technique: validation using field and satellite observations. *Natural Hazards* **105** (3), 2431–2453. https://doi.org/10.1007/s11069-020-04406-w.

Tehrany, M. S., Pradhan, B. & Jebur, M. N. 2013 Spatial prediction of flood susceptible areas using rule based decision tree (DT) and a novel ensemble bivariate and multivariate statistical models in GIS. *Journal of Hydrology* **504**, 69–79. https://doi.org/10.1016/j.jhydrol.2013.09.034.

Tehrany, M. S., Pradhan, B. & Jebur, M. N. 2014 Flood susceptibility mapping using a novel ensemble weights-of-evidence and support vector machine models in GIS. *Journal of Hydrology* **512**, 332–343. https://doi.org/10.1016/j.jhydrol.2014.03.008.

Tehrany, M. S., Pradhan, B., Mansor, S. & Ahmad, N. 2015 Flood susceptibility assessment using GIS-based support vector machine model with different kernel types. *Catena* **125**, 91–101. https://doi.org/10.1016/j.catena.2014.10.017.

Tehrany, M. S., Jones, S. & Shabani, F. 2019 Identifying the essential flood conditioning factors for flood prone area mapping using machine learning techniques. *Catena* **175** (December), 174–192. https://doi.org/10.1016/j.catena.2018.12.011.

Teng, J., Vaze, J., Dutta, D. & Marvanek, S. 2015 Rapid inundation modelling in large floodplains using LiDAR DEM. *Water Resources Management* **29** (8), 2619–2636. https://doi.org/10.1007/s11269-015-0960-8.

Towfiqul Islam, A. R. M., Talukdar, S., Mahato, S., Kundu, S., Eibek, K. U., Pham, Q. B., Kuriqi, A. & & Linh, N. T. T. 2021 Flood susceptibility modelling using advanced ensemble machine learning models. *Geoscience Frontiers* **12** (3). https://doi.org/10.1016/j.gsf.2020.09.006.

Ukumo, T. Y., Abebe, A., Lohani, T. K. & Edamo, M. L. 2022a Flood hazard mapping and analysis under climate change using hydro-dynamic model and RCPs emission scenario in Woybo River catchment of Ethiopia. *World Journal of Engineering*. https://doi.org/10.1108/WJE-07-2021-0410.

Ukumo, T. Y., Lohani, T. K., Edamo, M. L., Alaro, M. A., Ayele, M. A. & Borko, H. B. 2022b Application of Regional Climatic Models to Assess the Performance Evaluation of Changes on Flood Frequency in Woybo. 2022.

Vilasan, R. T. & Kapse, V. S. 2022 Evaluation of the prediction capability of AHP and F-AHP methods in flood susceptibility mapping of Ernakulam district (India). *Natural Hazards*. https://doi.org/10.1007/s11069-022-05248-4.

Wind, Y. & Saaty, T. L. 1980 Marketing applications of the analytic hierarchy process marketing applicatons of the analytic hierarchy process* Yoram Windt And Thomas L. Saaty. *Source: Management Science* **26** (7), 641–658.

Yang, A., Wang, C., Pang, G., Long, Y., Wang, L., Cruse, R. M. & Yang, Q. 2021 Gully erosion susceptibility mapping in highly complex terrain using machine learning models. *ISPRS International Journal of Geo-Information* **10** (10). https://doi.org/10.3390/ijgi10100680.

Zaharia, L., Costache, R. & Ioana-toroimac, G. 2019 *Mapping fl ood and fl ooding potential indices : a methodological approach to identifying areas susceptible to fl ood and fl ooding risk . Case study : the Prahova catchment (Romania)*. *April*. https://doi.org/10.1007/s11707-017-0636-1.

Zhao, R., Fu, P., Zhou, Y., Xiao, X., Grebby, S., Zhang, G. & Dong, J. 2022 Annual 30-m big lake maps of the Tibetan plateau in 1991–2018. *Scientific Data* **9** (1), 1–9. https://doi.org/10.1038/s41597-022-01275-9.

First received 24 June 2022; accepted in revised form 14 October 2022. Available online 1 November 2022